

Journal of Materials Chemistry A

Materials for energy and sustainability

Accepted Manuscript

This article can be cited before page numbers have been issued, to do this please use: S. Murmu, S. . Paul, S. Kapse , R. Thapa, S. Chattopadhyay, A. N, S. N. Jha, D. B and U. K. Ghora, *J. Mater. Chem. A*, 2021, DOI: 10.1039/D1TA00766A.



This is an Accepted Manuscript, which has been through the Royal Society of Chemistry peer review process and has been accepted for publication.

Accepted Manuscripts are published online shortly after acceptance, before technical editing, formatting and proof reading. Using this free service, authors can make their results available to the community, in citable form, before we publish the edited article. We will replace this Accepted Manuscript with the edited and formatted Advance Article as soon as it is available.

You can find more information about Accepted Manuscripts in the [Information for Authors](#).

Please note that technical editing may introduce minor changes to the text and/or graphics, which may alter content. The journal's standard [Terms & Conditions](#) and the [Ethical guidelines](#) still apply. In no event shall the Royal Society of Chemistry be held responsible for any errors or omissions in this Accepted Manuscript or any consequences arising from the use of any information it contains.

Unveiling the Genesis of the High Catalytic Activity in Nickel Phthalocyanine for Electrochemical Ammonia Synthesis

Shyamal Murmu¹, Sourav Paul¹, Samadhan Kapse², Ranjit Thapa², Santanu Chattopadhyay³, Abharana N⁴, Shambhu N. Jha⁴, Dibyendu Bhattacharyya⁴ and Uttam Kumar Ghorai^{1*}

¹Department of Industrial Chemistry & Applied Chemistry, Swami Vivekananda Research Centre, Ramakrishna Mission Vidyamandira, Belur Math, Howrah, 711202, India

²Department of Physics, SRM University – AP, Amaravati, Andhra Pradesh, 522502, India

³Rubber Technology Centre, Indian Institute of Technology, Kharagpur, 721302, India

⁴Atomic & Molecular Physics Division, Bhabha Atomic Research Centre, Mumbai, 400085, India

Corresponding author:

*Email: uttam.indchem@vidyamandira.ac.in

Abstract: Electrochemical ammonia synthesis by nitrogen reduction reaction (NRR) using economically efficient electrocatalyst can provide a substitute of Haber-Bosch process. However, identification of active sites responsible for the origination of catalytic activity in transition metal phthalocyanine is difficult task due its complex structure. Herein, density functional theory (DFT) is applied to identify the probable active sites of nickel phthalocyanine (NiPc) in NRR as well as origin of catalytic activity which is associated with d band center and density of states (DOS) of Ni in NiPc. Accordingly, the NiPc nanorods (NRs) were synthesized by solvothermal method in large scale and the chemically prepared NiPc NRs exhibit the NH₃ yield rate about 85 μg h⁻¹ mg_{cat}⁻¹ and Faradaic efficiency (FE) of 25 % at -0.3 V versus RHE. Moreover, the catalyst shows the long term stability till 30 hours while maintaining the NH₃ yield and FE. The isotopic labelling experiment and other control investigation led to validate the nitrogen source in NH₃ formation. This manifold study provides brand new insightful understanding on the active sites and origination of catalytic activity of NiPc for their NRR applications.

Keywords: Nickel Phthalocyanine, Nanorods, Nitrogen Reduction, Ammonia, d Band Center

Introduction

Ammonia is a crucial raw material widely used for various industrial sectors such as agricultural, chemical products and medicine.¹ Presently, Haber Bosch process is primarily used to manufacture ammonia, by the reaction of nitrogen and hydrogen at high pressure (150-200 atm) and high temperature (400-500°C), resulting in an energy intensive process with prodigious amount of carbon dioxide gas emission.²⁻³ From the sustainability point of view, it is necessary to develop energy efficient and eco-friendly process for ammonia production. Ammonia production by electrochemical route using electrocatalyst through nitrogen reduction reaction (NRR) at ambient condition is a budding alternative of industrial Haber-Bosch process.⁴⁻⁵ Yet, due to inert nature of the N≡N covalent bond and clashing hydrogen evolution reaction (HER) during NRR process, the evolution of efficient electrocatalyst with superior activity and selectivity is really challenging for the electrochemical conversion of di-nitrogen into ammonia.⁶⁻⁸ Nowadays, various potential electrocatalysts were developed by eminent research groups, including metals and metalloids⁹⁻²⁰, transition metal based sulfides, oxides, nitrides, carbides²¹⁻³³ and metal free³⁴⁻³⁶ catalyst. From the mentioned array of electrocatalyst, transition metals based catalysts are contemplated as a propitious electrocatalyst for NRR due to their synergism, where unoccupied d orbital metal center which can accept the lone-pair of electrons from nitrogen to boost the inception of metal-nitrogen bond and the electrons present at occupied d orbital in metal donate back to the antibonding orbital of nitrogen in order to weaken the N≡N bond.²⁵⁻²⁶ Simultaneously, there is a likelihood of the formation of metal-hydrogen bond by d orbital electron in transition metal, as a consequence it reduces the catalytic efficiency by enhancing the competitive HER. Contrarily non-metallic elements can be considered as nitrogen activation center in NRR due to their weak hydrogen adsorption of nonmetallic elements and abundant valence electrons.³⁶ Combination of transition metallic component along with active nonmetallic counterpart would be great interest and may aid in boosting the performance of NRR. Recently Prof. Hu and coworkers³⁷ reported iron phthalocyanine/carbon (FePc/C) as an active NRR electrocatalyst where the yield rate of NH₃ to be 10.25 μg h⁻¹ mg_{cat}⁻¹ at low potential of -0.3 V and FE of 10.50%. In our recent work, we synthesized pristine CoPc nanotubes by solvothermal method which showed the NH₃ yield 107.9 μg h⁻¹ mg_{cat}⁻¹ and FE of 27.7%.³⁸ Xu et al.³⁹ studied the electrocatalytic NRR activity of FePc/O-MWCNT (multiwall carbon nanotube) which showed the NH₃ yield 36 μg h⁻¹ mg_{cat}⁻¹ and FE of 9.73%. Their theoretical calculation proved

that NRR preferred alternating pathway over distal pathway. Mukherjee et al.⁴⁰ studied the NRR property of atomically dispersed NiN₃ site-rich catalyst showing an optimal NH₃ yield 115 $\mu\text{g cm}^{-2} \text{h}^{-1}$ and FE $21 \pm 1.9\%$ at neutral conditions. However, there is a lack in report on the NRR property of NiPc nanostructure. As electrochemical property is an integral interplay of surface activity and morphology, we firmly believe that superiority can be achieved through morphological tailoring, initiated recently.⁴¹ Nevertheless, the greatest challenge lies in precisely determining the origination of catalytic NRR activity of the electrocatalyst and the potent catalytic sites accountable for NRR are directly associated with precise selection of high performance electrocatalyst. The d band center is the well-known electronic descriptor to define the transition metals catalytic activity and it provides the information about the adsorption of intermediates as well as over potential during NRR.^{42, 43} Unfortunately, there is very few work to describe the nitrogen adsorption energy with d band center of the transition metal for NRR. Through this present work, we demonstrate a theory guided design of NiPc as NRR electrocatalyst. DFT study indicates that for NRR, the alternating pathway is preferred over distal pathway. We have discerned the several active sites and estimated d band center to correlate the charge transfer mechanism between N₂ and Ni during NRR. To realize the NRR catalytic activity of NiPc, we have prepared the NiPc nanorods by ethylene glycol assisted solvothermal route in large scale and further studied the NRR activity. The chemically synthesized NiPc nanorods showed the excellent NRR activities with NH₃ yield of 85 $\mu\text{g h}^{-1} \text{mg}_{\text{cat}}^{-1}$ at -0.3 V versus RHE and FE of 25%.

Results and discussion

DFT calculations were performed to trace the catalytic activity on pristine phthalocyanine (Pc) and nickel phthalocyanine (NiPc) towards NRR. According to reports, metal center is most active site in the metal-nitrogen-carbon (M-N-C) materials due to high charge transfer property and strong binding affinity towards adsorbed species.⁴⁴⁻⁴⁶ Therefore, our main focus is on Ni center as an active site on NiPc, whereas other sites are also consider for comparison. In **Figure 1**, we corroborated the free energy profile for NRR on Ni center via both distal and alternating reaction pathways. Here it is seen that the second step (*N₂ to *NNH) is the potential determining step (PDS) for both the pathways. Afterward we observed that the reaction step of *NNH undergoes to *NHNH due to the downhill free energy change of 0.28 eV, whereas the

step $*\text{NNH}$ to $*\text{NNH}_2$ shows uphill free energy change of 0.44 eV. It proposes that alternating pathways is more favourable than distal for NRR. For alternating pathway, we have shown the free-energy profile for negative applied potential ($U = -1.22$ V), where all the reaction steps are exothermic in nature (**Figure S1**).

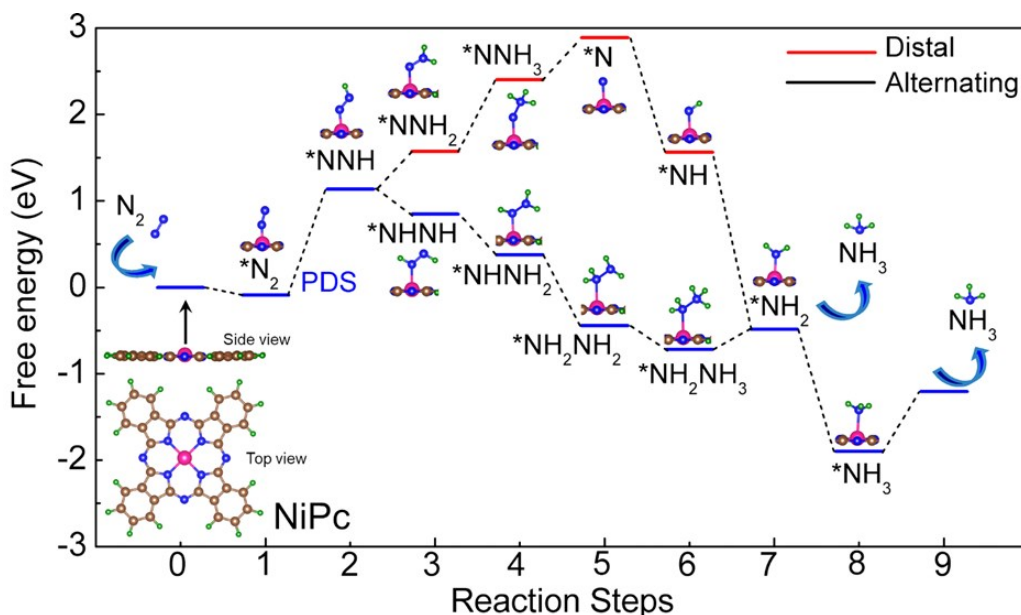


Figure 1 Demonstrate the free energy profile for nitrogen reduction reaction over NiPc considering alternating and distal pathways. Ni, C, N and H atoms are denoted with pink, grey, blue, and green sphere respectively. Intermediates are given in the inset. Dotted lines are used for indication purpose.

We have compared the free energy of N_2 adsorption and formation of NNH intermediate on Ni center of NiPc and carbon, pyrrolic-N3, pyrrolic-N2, and pyridinic-N1 of NiPc and Pc as shown in **Figure 2a** and **Figure S2**. For easier understanding of active sites on NiPc and Pc structures, we have provided **Figure S4**. It depicts that the weak binding of NNH intermediate on the carbon, pyrrolic-N3, pyrrolic-N2, pyridinic-N1 sites of NiPc/Pc is responsible for the higher free energy of NNH* and larger overpotential than the Ni center of NiPc (**Figure 2a** and **Figure S2**). The overpotential towards NRR on different active sites are obtained in the following order: Ni (1.22V) < pyrrolic-N3 (1.65V) < pyrrolic-N1 (1.77V) < pyridinic-N2 (1.789V) < carbon (2.29V) of NiPc structure. On Pc structure the overpotential values are pyrrolic-N2 (1.69V) < pyrrolic-N3 (1.70V) < pyridinic-N1 (1.78V) < carbon (2.19V). Furthermore, we corroborated the

free energy profile of HER to confirm the dominant reaction in NiPc and Pc systems. We have observed that the overpotentials for NRR on carbon/nitrogen sites of NiPc and Pc are higher than the overpotentials for HER (**Figure S3**). The result depicts overpotential for NRR on Ni as an active center is 1.22 V, which is in lower magnitude than hydrogen evolution overpotential (1.37 V). It demonstrates that the Ni center in NiPc is optimal active site to amplify the NRR by suppressing HER activity.

In order to comprehend the activity of metal center on NRR, we have correlated the N₂ and NNH adsorption energy with d band center. The d band center is well defined as the electronic descriptor for metal catalysts.^{42-43, 47-49} The d band center is estimated by using the following equation,

$$C_d = \frac{\int_{-\infty}^0 \rho_d E dE}{\int_{-\infty}^0 \rho_d dE} \quad (1)$$

Here, ρ_d is the partial density of states of d orbital, E is the energy in unit of eV and the Fermi level is set to zero. The calculated the value of d band center for Ni atom is -1.54 in the NiPc systems using the equation (1). The value of d band center is responsible for the charge transfer to the adsorbate and its adsorption energy. It exhibits that the d band center of metal atoms are affecting to the adsorption of intermediates as well as overpotential during NRR.

Furthermore, the d orbital density of state (DOS) of the Ni active site in NiPc is investigated to understand the adsorption of N₂ and NNH intermediates in NRR (**Figure 2b-2d**). It exhibits that the d band center in DOS of Ni is shifted towards negative direction after the adsorption of N₂ (-1.63 eV) and NNH intermediate (-2.23 eV). Similarly, the d orbital electron occupancy of Ni site is 8.52e decreased to 8.50e and 8.19e after the adsorption of N₂ and NNH respectively. It indicates that the charge is transferred from Ni active site to N₂ and NNH and that signify the adsorption of intermediates during NRR. In **Figure 2e & 2f**, the charge density difference analysis of NiPc with the adsorbed N₂ and NNH shows electron accumulation at the N-Ni bond that helps in the reduction reaction of nitrogen molecule. Therefore, Ni center on NiPc is a potential active site that should be accountable for the enhancement of NRR performance in phthalocyanine systems.

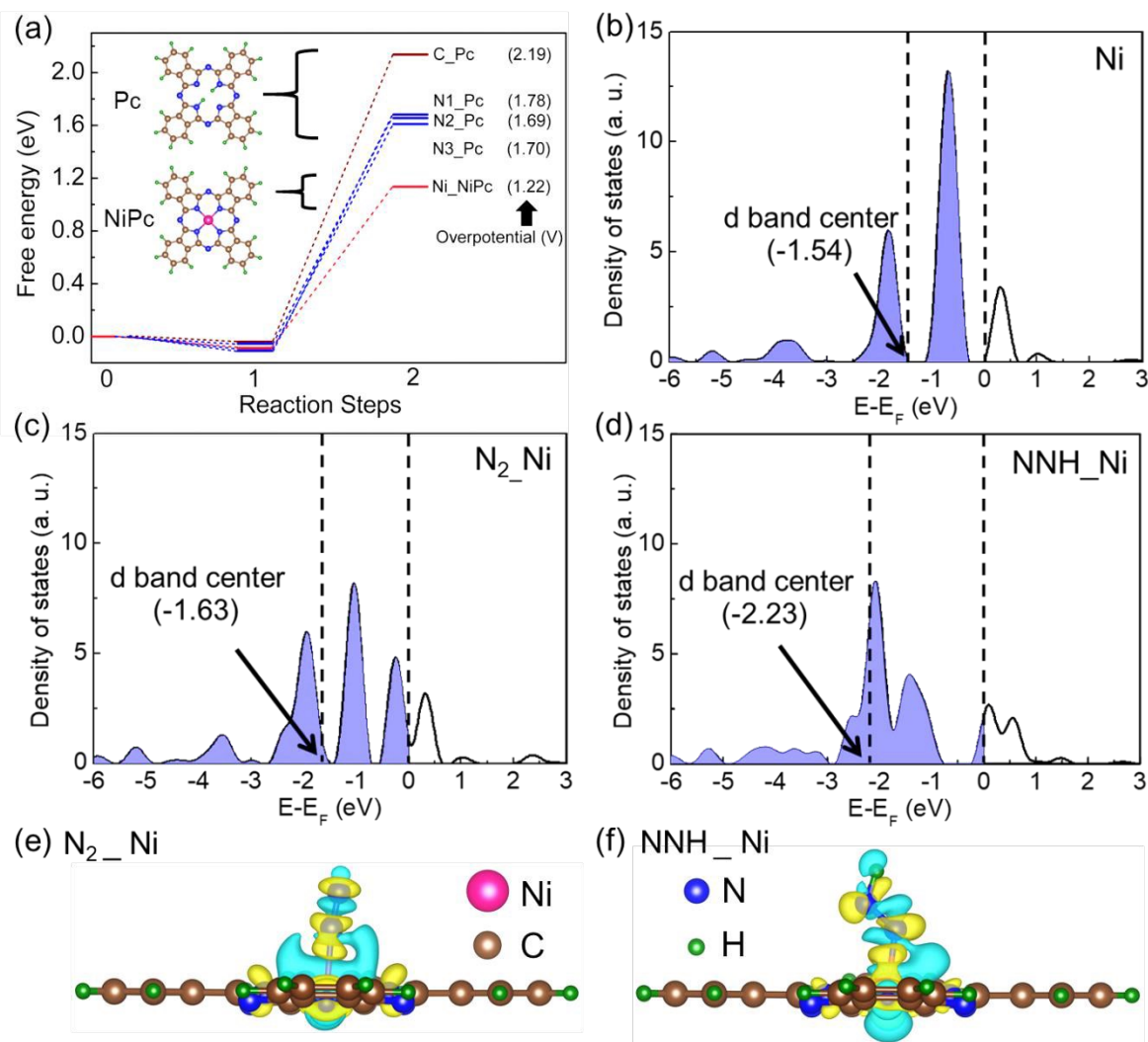


Figure 2 (a) Free-energy diagrams for N_2 and NNH adsorption on Ni center of NiPc and various sites of Pc (b) Shows the d orbital partial density of states of Ni center (c) Ni center after N_2 adsorption (d) Ni center after NNH adsorption of NiPc system. The Fermi level shown by dotted line at zero and the shaded area describes the d orbital occupancy. Demonstrate the charge density difference for (e) N_2 adsorbed NiPc and (f) NNH adsorbed NiPc. For easier understanding of the active sites (carbon, pyrrolic-N3, pyrrolic-N2, and pyridinic-N1 atoms), the Pc and NiPc structures with indicators are shown in Figure S4.

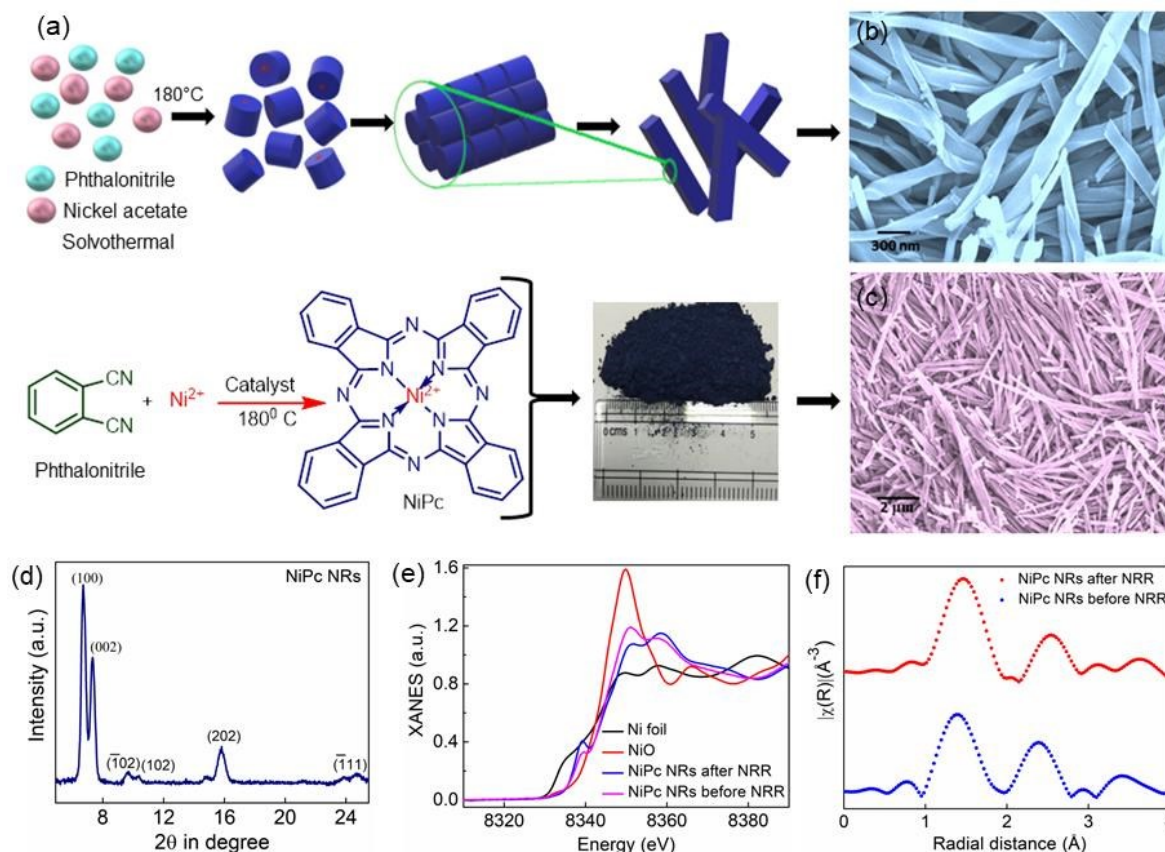


Figure 3 (a) Schematic formation process of NiPc 1D nanostructures and synthesis procedure; (b) FESEM image of NiPc NRs at higher magnification; (c) FESEM images of NiPc NRs; (d) XRD spectrum of NiPc NRs; (e) Normalized XANES spectra at Ni K-edge; (f) Experimental $\chi(R)$ vs. R data of NiPc NRs measured at Ni K-edge.

The schematic representation of the synthesis procedure of nanorods is depicted in the **Figure 3a**. Initially, small nanoclusters of NiPc are formed by the reaction of phthalonitrile, nickel acetate and catalyst in ethylene glycol solvent. With the increasing reaction time, NiPc nanoclusters are congregated through π - π interactions forming one dimensional rod like structure. The optical image of the chemically derived NiPc crystal is also shown in the **Figure 3a**. The FESEM images at different magnifications are shown in the **Figure 3b & 3c**. In **Figure 3b**, the microstructure of the NiPc shows large scale rod like morphology. The length and diameter of the chemically prepared NiPc are in the range of 2-12 μm and 50-250 nm

respectively. In **Figure 3d**, shows the XRD diffraction pattern of NiPc nanorods and all the peaks are well matched with the previous literature⁵⁰ assuring the pure phase formation. The major peaks appear at 6.72°, 7.38°, 9.60°, 10.31°, 15.88°, 24.92° values of 2θ , which corresponds to the reflections from (100), (002),(102),($\bar{1}02$), (202), ($\bar{1}11$) planes of NiPc respectively. The chemical composition and electronic structures of NiPc NRs were investigated by XPS. The survey scan of XPS spectrum demonstrates that major elements are Ni, N and C (depicted in **Figure S5**). In **Figure S6**, the peaks at 855.1 eV and 872.3 eV are commensurate with the electronic states of Ni $2p_{3/2}$ and $2p_{1/2}$ respectively.⁵⁰ The existence of satellite peak at 863.6 eV ensures the Ni (II) state in NiPc.^{50, 51} The high resolution spectrum of N1s is depicted in the **Figure S7**.

The synchrotron based X-ray absorption near-edge structure (XANES) and extended X-ray absorption fine structure (EXAFS) analysis were conducted to investigate the valence state(s) and local co-ordination environment of nickel in nickel pthalocyanine (NiPc) electrocatalyst during ENRR process and prior to it. The X-ray absorption position of Ni K-edge spectra of NiPc, before and after electrolysis was measured along with standard Ni foil and NiO, the X-ray absorption edge position of NiPc lies in between Ni and NiO, hence the valence state of 'Ni' in NiPc lies between 0 and +2 (**Figure 3e**). In XANES spectra, two distinct peaks at 8334 and 8339 eV are observed implying Ni-N₄ co-ordination in nickel pthalocyanine.⁵² The pre-edge small peak near 8334 eV commensurate with quadrupole allowed but dipole forbidden transition (1s to 3d), implicitly suggests orbital alloying of 3d and 4p of the nickel atom in nickel pthalocyanine,⁵³ whereas the shoulder peak at 8339 eV occurs for the 1s to 4p transition. The fourier transforms of EXAFS was observed at -0.3V in post and pre-electrolysis condition. The plot of EXAFS spectra in R co-ordinate space shows the following distinct peaks (**Figure 3f**): The first peak at ~1.44 Å represents the first shell Ni-N co-ordination bonds,⁵³ the second peak at ~2.47 Å corresponds to the Ni-C co-ordination while the small extended peak at ~0.79 Å arises due to superposition of peaks of Ni-N and Ni-C co-ordination.^{40, 54}

The electrochemical NRR activity of NiPc supported on GCE has been investigated in 0.1M HCl electrolyte using H-type electrochemical cell separated by a nafion 117 membrane under ambient condition (shown in **Figure S13** and detailed procedure in experimental section). The **Figure S14** demonstrates the linear sweep voltammetry (LSV) curves of NiPc NRs in N₂ (99.999%, ultra-high purity grade) purged solution and argon (Ar) gas purged solution with in

the potential range of -0.2 V to -0.6 V versus RHE and the enhancement of current density in N₂ solution which is starkly different than Ar solution within the potential range indicating the prominent NRR activity.²² **Figure 4a** shows the time dependent chronoamperometric curves of NiPc NRs in N₂ saturated solution at -0.2 V to -0.6 V versus RHE and corresponding UV-vis spectra with prominent absorption at 655 nm confirming the NRR activity is shown in **Figure 4b**. After NRR electrolysis for 6000 sec at different potential, the indophenol blue method and Watt & Chrisp method were employed to calculate the produced NH₃ (**SI 2 and Figure S15-S16**) and N₂H₄ respectively (**SI 3 and Figure S17-S18**). No by-product hydrazine (depicted in **Figure S19**) is formed during electrolysis, confirming the good selectivity of NiPc catalyst towards N₂ to NH₃. The calculated NH₃ yield and FE at various potential are presented in **Figure 4c**. The maximum NH₃ yield and FE of NiPc NRs at -0.3 V vs. RHE are 85 μg h⁻¹ mg_{cat}⁻¹ and 25 % respectively. The quantification of NH₃ yield was also carried out using ¹H NMR technique and the calibration plot shown in the supporting information (**Figure S20-S22 and SI4**). The NiPc NRs results in NH₃ yield and FE of 85.4 μg h⁻¹ mg_{cat}⁻¹ and 25.1% which are in unison with the result as obtained from UV-visible method.

Several control experiments were performed to verify the detected NH₃ was originated from NRR process or other source. First, pristine Glassy Carbon Electrode (GCE) shows the negligible amount of electrochemical NRR activity (**Figure S23**). Second, No NH₃ is detected for NiPc NRs in N₂ saturated open circuit potential (**Figure S23**) and Ar saturated electrolyte (**Figure S23**) at -0.3 V. Third, isotopic labelling experiment was performed with ¹⁵N₂ as feeding gas to produce ¹⁵NH₄⁺, hence it validates that ammonium is produced solely from N₂ source; as shown in **Figure 4e**. After electrolysis using ¹⁴N₂ and ¹⁵N₂ as feeding gas, ¹H NMR result showed triplet and doublet peaks due to formation of ¹⁴NH₄⁺ and ¹⁵NH₄⁺ ions, whereas no such peaks were observed when Ar was used as feeding gas.⁵⁵ The reusability and long term stability are the important parameters of an electrocatalyst for practical application. To reconnoitre the durability of NiPc catalyst, cycling test was executed in N₂ saturated 0.1 M HCl electrolyte at -0.3 V vs RHE. The NH₃ yield and corresponding FE was almost constant even after 5 consecutive cycles, implying the stable NRR electrocatalytic behaviour (**Figure 4d**). The long term electrocatalytic stability test of NiPc catalyst was performed at -0.3 V in N₂ saturated 0.1 M HCl electrolyte at different (6, 12, 18, 24 and 30 (hrs.)) testing periods. The catalyst demonstrated the steady and stable catalytic performance without significant change in current

density (shown in **Figure S25**). The obtained NH_3 yield and corresponding FE had negligible loss in compare with the initial cycles (**Figure 4f**).

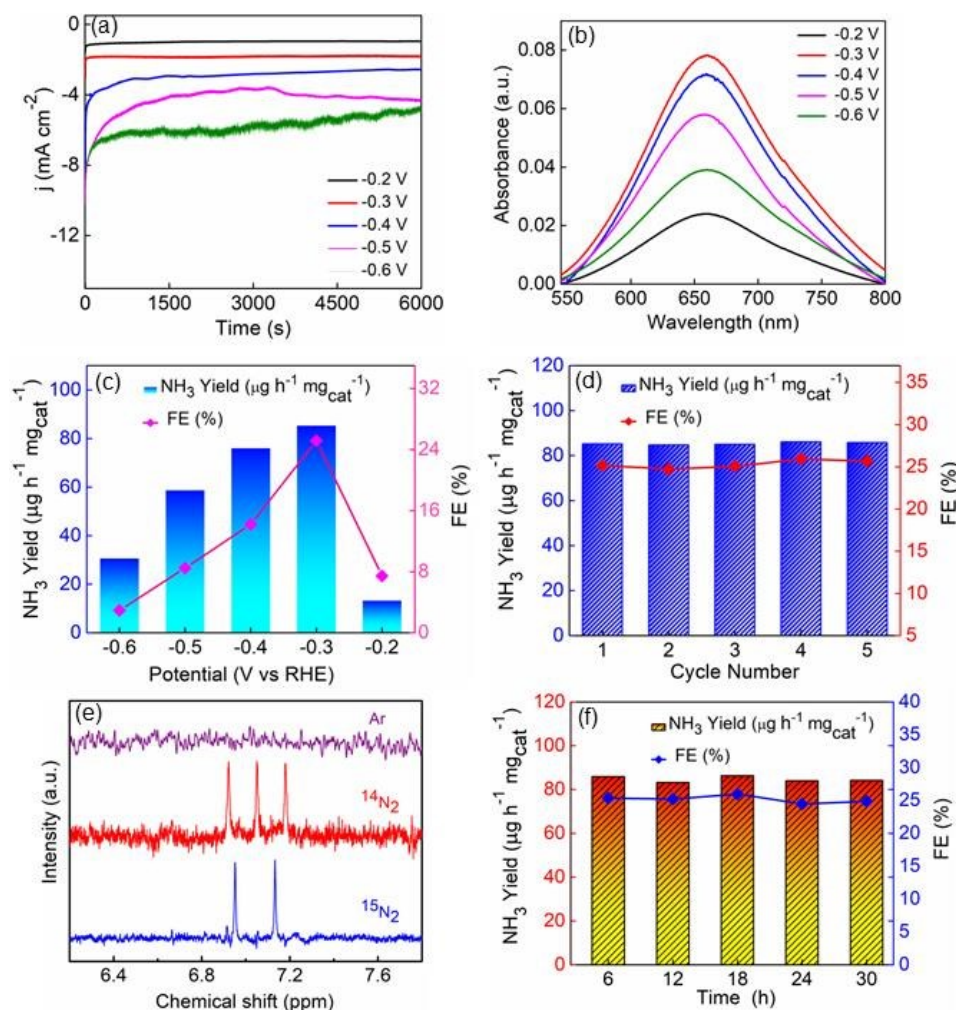


Figure 4:(a) Time reliant current density (J) curves for NiPc NRs at various potential;(b) UV-vis absorption spectra of the electrolytes stained with an indophenol indicator at different potential after 6000 sec NRR electrolysis; (c) Histogram of average NH_3 yield rate and corresponding Faradaic efficiency of NiPc NRs at different potential; (d) Recycling stability tests of NiPc NRs for NRR at -0.3 V vs RHE for five times; (e) ¹H NMR spectra of ¹⁴NH₄⁺ and ¹⁵NH₄⁺ produced from ENRR (at -0.3 V vs RHE) using ¹⁴N₂ and ¹⁵N₂ as the N₂ source; f) Histogram of average NH_3 yield rate and corresponding Faradaic efficiency of NiPc NRs at different time duration.

The reason for long term stable NRR activity of NiPc NRs occurs mainly due to the crystalline nature of NiPc NRs electrocatalyst. XPS survey scan profile of NiPc NRs after ENRR, concludes that the main constituents elements such as C, Ni and N are present in the catalyst (**Figure S27**). The additional peaks of Fluorine (F) arise because of the incorporation of Nafion binder in the NiPc prior to electrochemical testing. TEM image (**Figure S28**) of the post ENRR catalyst sample show that the one dimensional nanorod like morphology almost remains same after 30 hrs electrochemical test.

Conclusion: In summary, we have identified the several active sites of NiPc catalyst with the aid of DFT calculation which are responsible for N₂ adsorption and activation. Then, we have calculated the d band center and DOS of Ni to decipher the genesis of the catalytic activity together with charge transfer mechanism of Ni site to N₂* and NNH*. Accordingly, NiPc NRs have been prepared by low temperature solvothermal method in large scale and studied for electrocatalytic NRR. The chemically synthesized NiPc NRs show the high NH₃ yield and FE due to its presence of active sites and specific-selectivity. The long term stability and reusability of the NiPc NRs catalyst along with maintaining the NH₃ yield rate and FE make it demanding due to the practical applicability for electrochemical route to synthesize NH₃. These results help to develop the theory guided judicious approach of the NRR electrocatalyst to produce NH₃.

Experimental Section:

Computational details: All Geometry optimization calculations were performed using density functional theory (DFT) as implemented in the Vienna Ab initio Simulation Package (VASP).⁵⁶ The generalized gradient approximations (GGA) with Perdew–Burke–Ernzerhof (PBE) functional was employed to describe the exchange and correlation effect.⁵⁷ The electron-electron interaction was described by the projected augmented wave (PAW) method.⁵⁸ The plane-wave cutoff energy set to 450 eV for simulations of all systems and Brillouin zone sampled using a single point k (located at the gamma point). The optimizations were followed until the net energy less than 10⁻⁶ eV per atom and force converged to 0.01 eV/Å. To save calculation time, we considered frozen structures of NiPc and Pc (except active site). The vacuum in all directions of 15 Å is ready to avoid interaction between repeating images.

Theoretically, the overpotential (η) calculated through free energy profiles are utilized to estimate the catalyst activity towards nitrogen reduction reaction (NRR). The Gibbs free energy (G) for free energy profile is obtained by the accompanying equation, $G = E + ZPE - TS - neU$, where E is the energy calculated from DFT, ZPE is the zero-point energy, TS is the entropic term, n is number of electrons transferred and U is applied potential at the electrode.⁵⁹ However, the TS and ZPE of the adsorbed atoms/ions are negligible in comparison of gaseous phase at room temperature and pressure. In this case, the reported values of entropies and zero-point energies from chemical database (<https://janaf.nist.gov>) are taken for the free molecules and considered a situation at $U = 0$ V in the free energy profile.

Materials synthesis and characterization: All analytical grade reagents were used. For the preparation of NiPc, 8.6 mmol of phthalonitrile, 2.2 mmol of nickel acetate and specific amount of ammonium molybdate as catalyst were mixed with ethylene glycol solvent (Sigma Aldrich-99.8% pure) and stirred continuously for 20 minutes. Then the solution mixture was transferred to 90 ml Teflon lined autoclave and then placed in a heating oven for 4 hours at 180°C. After natural cooling to ambient temperature, the obtained material was washed with 1.0 N HCl, ethanol and mild hot water for several times to wash away the residual reagents. Eventually, the obtained blue colored precipitate was dried in an oven for 12 hours at 60°C. The phase purity and crystallinity of the synthesized NiPc NRs were confirmed by XRD technique using Bruker D-8 advanced Eco X-ray powder diffractometer (radiation Cu-K α with $\lambda=0.15404$ nm, current 25 mA, voltage 40 kV). The different chemical bonding in the NiPc nanostructures were examined by Shimadzu IRAffinity-1S FTIR spectrometer. Chemical compositions of NiPc crystals were examined by XPS using an OMICRON-0571 system. The electronic transitions of NiPc NRs were performed by UV-vis spectroscopy (Shimadzu UV-3600 Plus). The morphological structures of the chemically derived NiPc nanorods were observed by FESEM (Zeiss-Germany) and transmission electron microscope (FEG-TEM, JEOL-JEM 2100F).

Electrochemical measurements and working electrode preparation: The ENRR tests were carried out in dual compartment H-type cell in 0.1 M HCl with Nafion 117 membrane (Sigma Aldrich Chemical Reagent Co.) as a separating membrane. The amount of electrolyte in cathode and anode chamber was 20 ml respectively. In detail, Nafion 117 membrane was pre-treated in the following way, at first boiling in water at 80°C for an hour, then boiling in H₂O₂ aqueous

solution at 80°C for an hour, again water treatment at 80°C for an hour, then 3 hours treated with 0.5 M H₂SO₄ at 80°C, finally treated in water at 80°C for 6 hours. After rinsing it few times with triple distilled water, the membrane was used.

1 mg NiPc catalyst and 5 μL of Nafion solution (5 wt%) were dispersed in absolute isopropanol (100 μL) (Merck Co. Ltd.) with the help of sonication for a minute, followed by mixing for 5 minutes to form a homogeneous catalytic ink. Then, the 8 μL dispersion of homogeneous catalytic ink was loaded onto glassy carbon electrode (GCE) with effective area of 0.07 cm² and dried under ambient condition. The electrochemical experiments were performed with an electrochemical workstation (CHI760E) using three-electrode configuration, where catalyst coated on GCE acts as working electrode, Pt wire as counter electrode and Ag/AgCl (saturated in 3.5 M KCl) as reference electrode. All potentials values were converted to the reversible hydrogen electrode (RHE). The ENRR activity was checked by linear sweep voltammogram (LSV), measured in Ar or N₂ (99.999% ultra-high purity grade) saturated electrolyte (scan rate 50 mV s⁻¹), the provided LSV curves were the steady state curves obtained after several cycles.

Conflicts of interest

There are no conflicts of interest to declare.

ACKNOWLEDGEMENTS

UKG acknowledges the central DST-FIST programme (SR/FST/College-287/2015) for providing financial support. UKG thanks to DBT star college scheme (BT/HRD/11/036/2019) for funding. UKG acknowledges the Teachers Associateship for Research Excellence (TARE) scheme (TAR/2018/000763) of SERB, Govt. of India for research grant and fellowship. UKG also acknowledges Science & Technology and Biotechnology Department, Govt. of West Bengal for providing the financial support [199 (Sanc.)/ST/P/S&T/6G-12/2018]. R.T. thanks Board of Research in Nuclear Sciences (BRNS), India, for the financial support (Grant Nos. 37(2)/20/14/2018-BRNS/37144). RT thanks High Performance Computing Center, SRM IST for providing the computational facility. The authors wish to thank Ashadul Adalder and Dr. Subhajit Saha for their technical assistance.

AUTHOR CONTRIBUTIONS:

UKG proposed the idea and designed the experiments. SM and UKG synthesized the materials and performed XRD, FTIR, UV-vis. SP, SM and UKG carried out all the electrochemical measurements and analyzed the results. SK and RT performed the DFT calculation. RT, SK, SM and UKG analyzed the DFT results. SC and SM did the morphological characterization. SP, SM and UKG analyzed the NMR data. AN, SJ and DB performed the XANES and EXAFS experiment. DB, AN, SP, SM and UKG analyzed XANES and EXAFS results. UKG wrote the original manuscript. SP, RT, AN, SM and SC co-wrote the manuscript. All authors approved the final version of the manuscript. UKG supervised the entire project.

REFERENCES

1. A. Good, *Science*, 2018, **359**, 869-870.
2. J. G. Chen, R. M. Crooks, L. C. Seefeldt, K. L. Bren, R. Morris Bullock, M. Y. Darensbourg, P. L. Holland, B. Hoffman, M. J. Janik, A. K. Jones, M. G. Kanatzidis, P. King, K. M. Lancaster, S. V. Lymar, P. Pfromm, W. F. Schneider and R. R. Schrock, *Science* (80-.), DOI:10.1126/science.aar6611.
3. K. A. Brown, D. F. Harris, M. B. Wilker, A. Rasmussen, N. Khadka, H. Hamby, S. Keable, G. Dukovic, J. W. Peters, L. C. Seefeldt and P. W. King, *Science* (80-.),, 2016, **352**, 448–450.
4. C. Tang and S. Z. Qiao, *Chem. Soc. Rev.*, 2019, **48**, 3166–3180.
5. X. Zhu, S. Mou, Q. Peng, Q. Liu, Y. Luo, G. Chen, S. Gao and X. Sun, *J. Mater. Chem. A*, 2020, **8**, 1545–1556.

6. G. F. Chen, S. Ren, L. Zhang, H. Cheng, Y. Luo, K. Zhu, L. X. Ding and H. Wang, *Small Methods*, 2019, **3**, 1–20.
7. G. F. Chen, X. Cao, S. Wu, X. Zeng, L. X. Ding, M. Zhu and H. Wang, *J. Am. Chem. Soc.*, 2017, **139**, 9771–9774.
8. T. Wu, H. Zhao, X. Zhu, Z. Xing, Q. Liu, T. Liu, S. Gao, S. Lu, G. Chen, A. M. Asiri, Y. Zhang and X. Sun, *Adv. Mater.*, 2020, **32**, 1–8.
9. M. M. Shi, D. Bao, S. J. Li, B. R. Wulan, J. M. Yan and Q. Jiang, *Adv. Energy Mater.*, 2018, **8**, 1–6.
10. D. Bao, Q. Zhang, F. L. Meng, H. X. Zhong, M. M. Shi, Y. Zhang, J. M. Yan, Q. Jiang and X. B. Zhang, *Adv. Mater.*, 2017, **29**, 1604799.
11. Y. Wang, M. Shi, D. Bao, F. Meng, Q. Zhang, Y. Zhou, K. Liu, Y. Zhang, J. Wang, Z. Chen, D. Liu, Z. Jiang, M. Luo, L. Gu, Q. Zhang, X. Cao, Y. Yao, M. Shao, Y. Zhang, X. Zhang, J. G. Chen, J. Yan and Q. Jiang, *Angew. Chemie*, 2019, **131**, 9564–9569.
12. X. Zhang, T. Wu, H. Wang, R. Zhao, H. Chen, T. Wang, P. Wei, Y. Luo, Y. Zhang and X. Sun, *ACS Catal.*, 2019, **9**, 4609–4615.
13. D. Yao, C. Tang, L. Li, B. Xia, A. Vasileff, H. Jin, Y. Zhang and S. Z. Qiao, *Adv. Energy Mater.*, 2020, **10**, 1–8.
14. X. Liu, Y. Jiao, Y. Zheng and S. Z. Qiao, *ACS Catal.*, 2020, **10**, 1847–1854.
15. H. Tao, C. Choi, L. X. Ding, Z. Jiang, Z. Han, M. Jia, Q. Fan, Y. Gao, H. Wang, A. W. Robertson, S. Hong, Y. Jung, S. Liu and Z. Sun, *Chem*, 2019, **5**, 204–214.
16. J. Wang, B. Huang, Y. Ji, M. Sun, T. Wu, R. Yin, X. Zhu, Y. Li, Q. Shao and X. Huang, *Adv. Mater.*, 2020, **32**, 1–9.
17. C. Yang, B. Huang, S. Bai, Y. Feng, Q. Shao and X. Huang, *Adv. Mater.*, 2020, **32**, 1–10.

18. W. Tong, B. Huang, P. Wang, L. Li, Q. Shao and X. Huang, *Angew. Chemie - Int. Ed.*, 2020, **59**, 2649–2653.
19. Z. H. Xue, S. N. Zhang, Y. X. Lin, H. Su, G. Y. Zhai, J. T. Han, Q. Y. Yu, X. H. Li, M. Antonietti and J. S. Chen, *J. Am. Chem. Soc.*, 2019, **141**, 14976–14980.
20. Y. C. Hao, Y. Guo, L. W. Chen, M. Shu, X. Y. Wang, T. A. Bu, W. Y. Gao, N. Zhang, X. Su, X. Feng, J. W. Zhou, B. Wang, C. W. Hu, A. X. Yin, R. Si, Y. W. Zhang and C. H. Yan, *Nat. Catal.*, 2019, **2**, 448–456.
21. L. Zhang, X. Ji, X. Ren, Y. Ma, X. Shi, Z. Tian, A. M. Asiri, L. Chen, B. Tang and X. Sun, *Adv. Mater.*, 2018, **30**, 2–7.
22. X. Li, T. Li, Y. Ma, Q. Wei, W. Qiu, H. Guo, X. Shi, P. Zhang, A. M. Asiri, L. Chen, B. Tang and X. Sun, *Adv. Energy Mater.*, 2018, **8**, 1–8.
23. J. Han, Z. Liu, Y. Ma, G. Cui, F. Xie, F. Wang, Y. Wu, S. Gao, Y. Xu and X. Sun, *Nano Energy*, 2018, **52**, 264–270.
24. T. Wu, X. Zhu, Z. Xing, S. Mou, C. Li, Y. Qiao, Q. Liu, Y. Luo, X. Shi, Y. Zhang and X. Sun, *Angew. Chemie - Int. Ed.*, 2019, **58**, 18449–18453.
25. J. Zhang, Y. Ji, P. Wang, Q. Shao, Y. Li and X. Huang, *Adv. Funct. Mater.*, 2020, **30**, 1–8.
26. H. Cheng, L. X. Ding, G. F. Chen, L. Zhang, J. Xue and H. Wang, *Adv. Mater.*, 2018, **30**, 1–7.
27. H. Jin, L. Li, X. Liu, C. Tang, W. Xu, S. Chen, L. Song, Y. Zheng and S. Z. Qiao, *Adv. Mater.*, 2019, **31**, 1–8.
28. X. Liu, Y. Jiao, Y. Zheng, M. Jaroniec and S. Z. Qiao, *J. Am. Chem. Soc.*, 2019, **141**, 9664–9672.

29. S. J. Li, D. Bao, M. M. Shi, B. R. Wulan, J. M. Yan and Q. Jiang, *Adv. Mater.*, 2017, **29**, 1–6.
30. M. M. Shi, D. Bao, B. R. Wulan, Y. H. Li, Y. F. Zhang, J. M. Yan and Q. Jiang, *Adv. Mater.*, 2017, **29**, 2–7.
31. K. Chu, Y. P. Liu, Y. B. Li, H. Zhang and Y. Tian, *J. Mater. Chem. A*, 2019, **7**, 4389–4394.
32. K. Chu, Y. H. Cheng, Q. Q. Li, Y. P. Liu and Y. Tian, *J. Mater. Chem. A*, 2020, **8**, 5865–5873.
33. K. Chu, Y. ping Liu, Y. biao Li, Y. li Guo, Y. Tian and H. Zhang, *Appl. Catal. B Environ.*, 2020, **264**, 118525.
34. W. Qiu, X. Y. Xie, J. Qiu, W. H. Fang, R. Liang, X. Ren, X. Ji, G. Cui, A. M. Asiri, G. Cui, B. Tang and X. Sun, *Nat. Commun.*, 2018, **9**, 1–8.
35. Y. Yang, L. Zhang, Z. Hu, Y. Zheng, C. Tang, P. Chen, R. Wang, K. Qiu, J. Mao, T. Ling and S. Z. Qiao, *Angew. Chemie - Int. Ed.*, 2020, **59**, 4525–4531.
36. L. Zhang, L. Ding, G. Chen, X. Yang and H. Wang, *Angew. Chemie*, 2019, **131**, 2638–2642.
37. C. He, Z. Y. Wu, L. Zhao, M. Ming, Y. Zhang, Y. Yi and J. S. Hu, *ACS Catal.*, 2019, **9**, 7311–7317.
38. U. K. Ghorai, S. Paul, B. Ghorai, A. Adalder, S. Kapse, R. Thapa, A. Nagendra, A. Gain, *ACS Nano*, 2021, **15**, 5230–5239.
39. F. Xu, L. Zhang, X. Ding, M. Cong, Y. Jin, L. Chen and Y. Gao, *Chem. Commun.*, 2019, **55**, 14111–14114.

40. S. Mukherjee, X. Yang, W. Shan, W. Samarakoon, S. Karakalos, D. A. Cullen, K. More, M. Wang, Z. Feng, G. Wang and G. Wu, *Small Methods*, 2020, **4**, 1–11.
41. K. P. Madhuri, N. S. John, *Applied Surface Science*, 2018, **449**, 528-536.
42. B. Hammer and J. K. Norskov, *Nature*, 1995, **376**, 238–240.
43. T. Deng, C. Cen, H. Shen, S. Wang, J. Guo, S. Cai and M. Deng, *J. Phys. Chem. Lett.*, 2020, **11**, 6320–6329.
44. N. L. Tran and A. C. Kummel, *J. Chem. Phys.*, 2007, **127** (21), DOI:10.1063/1.2799988.
45. A. Mugarza, R. Robles, C. Krull, R. Korytár, N. Lorente and P. Gambardella, *Phys. Rev. B - Condens. Matter Mater. Phys.*, 2012, **85**, 1–13.
46. M. Wang, S. Liu, T. Qian, J. Liu, J. Zhou, H. Ji, J. Xiong, J. Zhong and C. Yan, *Nat. Commun.*, 2019, **10**, 1–8.
47. I. Takigawa, K. I. Shimizu, K. Tsuda, and S. Takakusagi, *RSC Adv.*, 2016, **6**, 52587-52595.
48. H. Sun, M. Wang, X. Du, Y. Jiao, S. Liu, T. Qian, Y. Yan, C. Liu, M. Liao, Q. Zhang, and L. Meng, *J. Mater. Chem. A*, 2019, **7**, 20952-20957.
49. H. Guo, L. Li, X. Wang, G. Yao, H. Yu, Z. Tian, B. Li, and L. Chen, *ACS Appl. Mater. Interfaces*, 2019, **11**, 36506-36514.
50. X. Wang, W. Wu, H. Ju, T. Zou, Z. Qiao, H. Gong and H. Wang, *Mater. Res. Express*, 2016, **3**, 1–10.
51. U. K. Ghorai, S. Das, S. Saha, N. Mazumder, D. Sen and K. K. Chattopadhyay, *Dalt. Trans.*, 2014, **43**, 9260–9266.
52. H. B. Yang, S. F. Hung, S. Liu, K. Yuan, S. Miao, L. Zhang, X. Huang, H.-Y. Wang, W.

- Cai, R. Chen, J. Gao, X. Yang, W. Chen, Y. Huang, H. M. Chen, C. M. Li, T. Zhang, B. Liu, *Nat. Energy*, 2018, **3**, 140-147.
53. T. Zheng, K. Jiang, N. Ta, Y. Hu, J. Zeng, J. Liu and H. Wang, *Joule*, 2019, **3**, 265–278.
54. C. Zhao, X. Dai, T. Yao, W. Chen, X. Wang, J. Wang, J. Yang, S. Wei, Y. Wu, Y. Li, *J. Am. Chem. Soc.*, 2017, **139**, 8078-8081.
55. S. Z. Andersen, V. Čolić, S. Yang, J. A. Schwalbe, A. C. Nielander, J. M. McEnaney, K. Enemark-Rasmussen, J. G. Baker, A. R. Singh and B. A. Rohr, et al., *Nature*, 2019, **570**, 504–508.
56. G. Kresse and J. Furthmüller, *Comput. Mater. Sci.*, 1996, **6**, 15–50.
57. J. P. Perdew, K. Burke and M. Ernzerhof, *Phys. Rev. Lett.*, 1996, **77**, 3865–3868.
58. P. E. Blöchl, *Phys. Rev. B*, 1994, **50**, 17953–17979.
59. S. Sinthika, U. V. Waghmare and R. Thapa, *Small*, 2018, **14**, 1–10.